Inorg. Chem. **2008**, *47*, 9766−9772

Low-Temperature and Template-Free Synthesis of $ZnIn_2S_4$ Microspheres

Zhixin Chen, Danzhen Li,* Wenjuan Zhang, Chun Chen, Wenjuan Li, Meng Sun, Yunhui He, and Xianzhi Fu*

Research Institute of Photocatalysis, State Key Laboratory Breeding Base of Photocatalysis, Fuzhou University, Fuzhou, 350002, P. R. China

Received April 26, 2008

Porous $ZnIn_2S_4$ microspheres have been successfully synthesized by means of a facile thermal solution method at 353 K. This method was a simple route that involved low temperature, no templates, no catalysts, no surfactants, or organic solvents. Scanning electron microscopy, transmission electron microscopy, high-resolution transmission electron microscopy, X-ray diffraction, energy-dispersive X-ray spectroscopy, X-ray photoelectron spectroscopy, nitrogen sorption analysis, and a UV−vis spectrophotometer were used to characterize the products. The results demonstrated that the microspheres, which were composed of many $ZnIn_2S_4$ single crystal nanosheets, underwent the Oswald ripening and self-assembly processes. A morphology formation mechanism has been proposed and discussed. The porous $ZnIn_2S_4$ product showed an enhancing visible-light photocatalytic activity for methyl orange degradation. The as-grown architectures may have potential applications in solar energy conversion, environmental remediation, and advanced optical/electric nanodevices.

Introduction

$ZnIn_2S_4$, an important semiconducting material of ternary chalcogenides, has attracted considerable attention because of its outstanding electrical and optical properties.[1−5] Various $ZnIn_2S_4$ nanostructures have been successfully fabricated by a variety of methods owing to its important potentials in photocatalysis, charge storage, electrochemical recording, and thermoelectricity.[1,6−9] For instance, Lei et al. reported a hydrothermal synthesis of $ZnIn_2S_4$ nanoparticles at 453 K and examined their potential application for photocatalytic water reduction under visible-light irradiation.[6] Intriguing $ZnIn_2S_4$ nanotubes, nanoribbons, nanowires, and microspheres have been prepared by Gou et al. on the basis of hydrothermal/solvothermal processes at more than 433 K.[10] Recently, hierarchically porous $ZnIn_2S_4$ submicrospheres have been synthesized by Hu et al. through a microwave−solvothermal approach at 473 K and showed enhanced visible-light photocatalytic activity for methylene blue degradation.[8]

These studies were important for understanding the formation of complex $ZnIn_2S_4$ microspheres and their potential applications in photocatalysis. Despite these advances, however, these methods mentioned above relied on relative higher temperature and special equipments or reagents. Some needed either Teflon-lined stainless-steel autoclave[6,10,11] or a microwave system with Teflon-lined double-walled digestion vessel.[8] Some depended on organic solvents (ethylene glycol,[8] pyridine,[10] ethanol[11]) as the reaction mediates, and some demanded the surfactants (cetyltrimethylammonium bromide or poly (ethylene glycol))[10,11] as templates. In summary, these methods were not simple. Therefore, further development of the direct fabrication of $ZnIn_2S_4$ with a low temperature, template-free, and facile synthetic method is quite necessary. In particular, to the best of our knowledge, there has been no report on the low temperature synthesis of $ZnIn_2S_4$.

* To whom correspondence should be addressed. Tel and Fax: (+86)591-83779256, E-mail: dzli@fzu.edu.cn (L.D.), xzfu@fzu.edu.cn (F.X.).

(1) Seo, W. S.; Otsuka, R.; Okuno, H.; Ohta, M.; Koumoto, K. *J. Mater. Res.* **1999**, *14*, 4176–4181.
(2) Anagnostopoulos, A.; Spyridelis, I. *Phys. Status Solidi A* **1981**, *66*, K127–K130.
(3) Zhitar, V. F.; rievskaya, N. I.; Arama, E. D. *Inorg. Mater.* **1992**, *28*, 1623–1624.
(4) Giorgianni, U.; Grasso, V.; Mondio, G.; Saitta, G. *Phys. Lett. A* **1978**, *68*, 247–248.
(5) Bosacchi, A.; Bosacchi, B.; Franchi, S.; Hernande, L. *Solid State Commun.* **1973**, *13*, 1805–1809.
(6) Lei, Z. B.; You, W. S.; Liu, M. Y.; Zhou, G. H.; Takata, T.; Hara, M.; Domen, K.; Li, C. *Chem. Commun.* **2003**, 2142–2143.
(7) Romeo, N.; Vigil, O. *Phys. Status Solidi A* **1972**, *10*, 447–453.
(8) Hu, X. L.; Yu, J. C.; Gong, J. M.; Li, Q. *Cryst. Growth Des.* **2007**, *7*, 2444–2448.
(9) Sriram, M. A.; McMichael, P. H.; Waghray, A.; Kumta, P. N.; Misture, S.; Wang, X. L. *J. Mater. Sci.* **1998**, *33*, 4333–4339.
(10) Gou, X. L.; Cheng, F. Y.; Shi, Y. H.; Zhang, L.; Peng, S. J.; Chen, J.; Shen, P. W. *J. Am. Chem. Soc.* **2006**, *128*, 7222–7229.

10.1021/ic800752t CCC: $40.75
Published on Web 10/10/2008

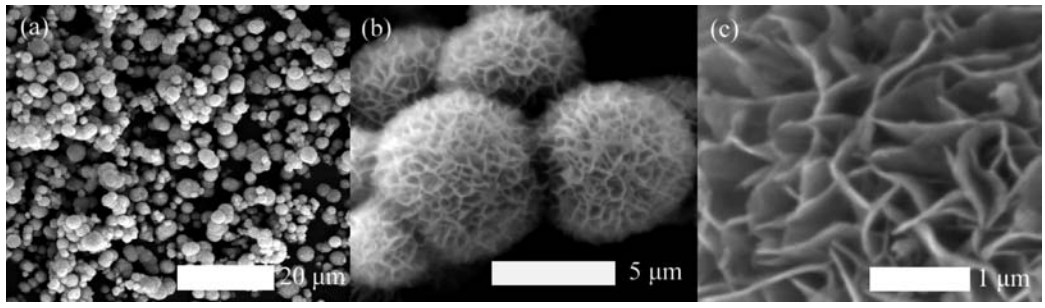

Figure 1. (a) Low-magnification and (b, c) high-magnification SEM images of the as-prepared porous $ZnIn_2S_4$ microspheres.

Herein, a template-free synthesis of $ZnIn_2S_4$ microspheres at low temperature in aqueous solution was reported. Compared with the methods mentioned above, this synthetic procedure has the advantages of simplicity (without any special equipments, organic solvents or templates) and low temperature (353 K). The mechanism related to the phase formation of $ZnIn_2S_4$ was proposed and discussed. Furthermore, the application of $ZnIn_2S_4$ in photocatalytic degradation of methyl orange (MO) has been investigated. As expected, the resulting porous $ZnIn_2S_4$ product showed efficient visible-light photocatalytic degradation of MO.

Experimental Section

Synthesis. All chemicals were analytical grade and used as received without further purification. In a typical reaction, $ZnCl_2$ (1 mmol) and $InCl_3 \cdot 4H_2O$ (2 mmol) were added by a stoichiometric ratio, and excessive thioacetamide (TAA, 6 mmol) was dissolved in a flask containing 100 mL deionized water, adjusting the solution to pH 2.5 by hydrochloric acid, and then the flask was put into a 353 K water bath for 6 h with no stirring. After the reaction was completed, the flask was cooled to room temperature naturally. The product was collected by centrifugation and then washed several times with deionized water and absolute ethanol. The final sample was dried at 333 K for 6 h in a vacuum for characterization. Furthermore, some reaction parameters that were influential to synthesis such as heating time, the pH value and the amounts of TAA were investigated to better understand the reaction mechanisms.

Characterization. The X-ray diffraction (XRD) patterns, obtained on a Bruker D8 Advance X-ray diffractometer using Cu $K\alpha_1$ irradiation (λ = 1.5406 Å) were used to identify the phase constitutions in samples. The accelerating voltage and the applied current were 40 kV and 40 mA, respectively. UV−vis diffuse reflectance spectra were obtained by a Varian cary 500 UV−vis-NIR spectrophotometer and were converted from reflection to absorption by the Kubelka−Munk method. The specific surface area and porosities of the samples were measured by N_2 adsorption at 77 K on Micrometritics ASAP2020 analyzer and calculated by the Brunauer−Emmett−Teller (BET) method. All of the samples were degassed at 343 K overnight prior to BET measurements. The general morphology of the products was examined by scanning electron microscopy (SEM) on a JEOL JSM 6700F instrument operated at 20 kV and equipped with an energy-dispersive X-ray analyzer (Phoenix). The morphology and microstructure of the composite were further investigated by transmission electron microscopy (TEM) and high-resolution TEM (HRTEM) using a JEOL JEM 2010F microscope working at 200 kV. X-ray photoelectron spectroscopy (XPS) analysis was conducted on a ESCALAB 250 photoelectron spectroscopy (Thermo Fisher Scientific) at 3.0×10^{-10} mbar with monochromatic Al Kα radiation (E = 1486.2 eV).

Photocatalytic Activity Measurements. The photocatalytic degradation of MO was carried out in an aqueous solution at ambient temperature. Briefly, a 40 mg of $ZnIn_2S_4$ was suspended in a 80 mL aqueous solution containing 10 ppm MO. The system was cooled by fan and circulating water to maintain the room temperature. Prior to irradiation, the suspension was magnetically stirred in the dark to ensure establishment of an adsorption−desorption equilibrium. The visible-light source system consisted of a 500 W tungsten−halogen lamp (Philips Electronics) and a composited cutoff filters that restricted the illumination to a range of 420−800 nm. Photocatalytic degradation was monitored by measuring the absorbance of solution using a Varian Cary 50 Scan UV−vis spectrophotometer.

Results

$ZnIn_2S_4$ was successfully synthesized through a simple approach employing low-temperature (353 K) reaction of $ZnCl_2$, $InCl_3$, and TAA in aqueous solution. The influence of synthesis conditions on the morphology of the product was studied by altering the pH value of solution, amount of TAA, and heating time.

The morphology of the as-synthesized $ZnIn_2S_4$ was investigated by SEM. Part a of Figure 1 showed the overall morphology of the product. It revealed that the product was composed of a large quantity of microspheres with an average diameter of about 3−7 μm. Part b of Figure 1 showed the SEM image of the product at a higher magnification and indicated these $ZnIn_2S_4$ microspheres had a unique marigold-like spherical superstructure. It was observed that the microsphere was composed of numerous nanosheets, as showed in part c of Figure 1, and macropores or mesopores may be formed among these nanosheets.

Further investigation was carried out by TEM to reveal the structure of such complex microsphere. Part a of Figure 2 presented an individual microsphere with a zigzag circle, in accordance with the SEM images (such as part b of Figure 1). In the picture, the color of nanosheets which were vertical to the picture was dark, whereas the color of parallel nanosheets was light. Part b of Figure 2 was the enlarged TEM image of the area marked by a red rectangle in part a of Figure 2. Obviously, some unequal nanosheets that assembled into fringes of microsphere can be seen. The selected-area electron diffraction (SAED) pattern of this part was showed in the inset. The pattern exhibited a clear hexagonal dif-

(11) Kale, B. B.; Baeg, J. O.; Lee, S. M.; Chang, H. J.; Moon, S. J.; Lee, C. W. *Adv. Funct. Mater.* **2006**, *16*, 1349–1354.

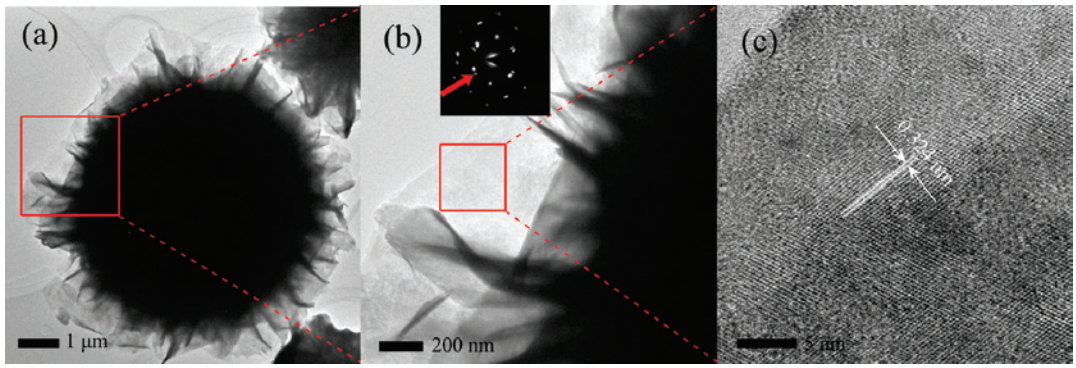

Figure 2. (a) Low-magnification, (b) high-magnification, and (c) high-resolution TEM images of the synthesized $ZnIn_2S_4$.

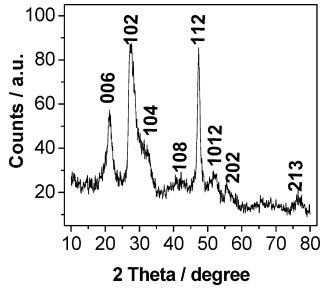

Figure 3. Typical XRD pattern of the as-prepared $ZnIn_2S_4$ microspheres.

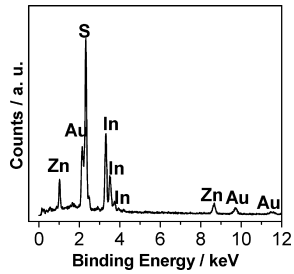

Figure 4. Typical EDS pattern of the as-prepared $ZnIn_2S_4$ microspheres.

fraction spot array and could be indexed to the single crystalline $ZnIn_2S_4$. Observed carefully, there was a small spot which marked by the red arrow beside big hexagonal diffraction spot. This was because there was double layer of $ZnIn_2S_4$ single crystalline in this area. The HRTEM image showed in part c of Figure 2 was investigated on the fringe part of a thin plate area (marked by a red rectangle in part b of Figure 2). The lattice interplanar spacing was measured to be 0.324 nm, corresponding to the (102) plane of hexagonal $ZnIn_2S_4$.

The phase and crystallographic structure of the products were determined by XRD. Figure 3 showed the typical XRD pattern of the as-prepared $ZnIn_2S_4$ product. Although their reaction conditions were different, the XRD patterns of all of the samples presented almost same profiles, and all of the diffraction peaks could be indexed to a hexagonal phase of $ZnIn_2S_4$, which was in agreement with the JCPDS No. 65−2023. No other impurities, such as binary sulfides, oxides, or organic compounds related to reactants, were detected by XRD analysis. The typical energy dispersive spectrometer (EDS) result (Figure 4) also demonstrated that the product was composed of only zinc, indium, and sulfur, in addition to the gold peaks came from sputtered. To further investigate

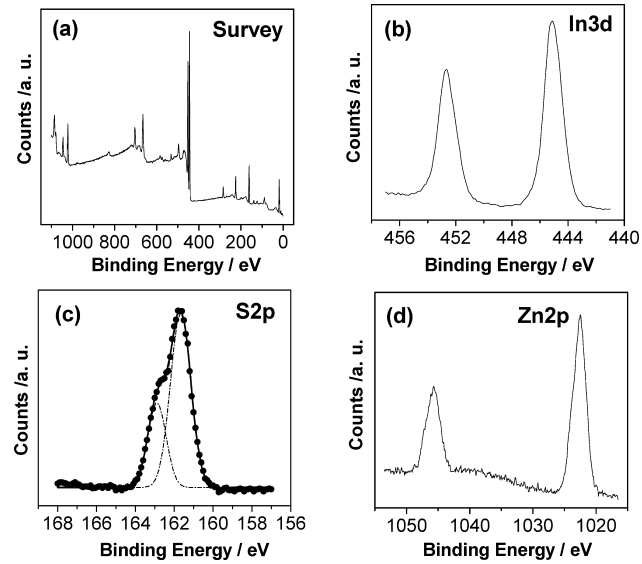

Figure 5. XPS spectra of the as-obtained $ZnIn_2S_4$ microspheres: (a) survey XPS spectrum and (b−d) high-resolution spectra of In3d, S2p, and Zn2p.

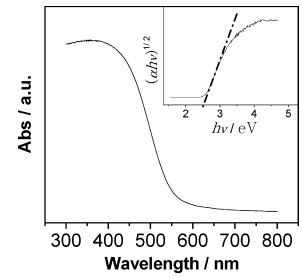

Figure 6. UV−vis diffuse reflectance spectrum of $ZnIn_2S_4$ product. The insert showed the plots of $(\alpha h\nu)^2$ vs $h\nu$.

the surface compositions and chemical state of the as-prepared $ZnIn_2S_4$ products, XPS was carried out, and the results were showed in Figure 5. The binding energies obtained in the XPS analysis were corrected for specimen charging by referencing carbon 1s to 284.5 eV. As shown in parts b−d of Figure 5, the core lines were fixed at 445.1 eV (In3d5/2), 161.7 eV (S2p3/2) and 1022.1 eV (Zn2p3/2). For In3d, S2p, and Zn2p, the spin orbit separations (Δ) were 7.5, 1.2, and 23.0 eV, and the ratios of two peak area were 2:3, 1:2 and 1:2, respectively. These results showed that the chemical states of the sample were In^{3+}, S^{2-}, and Zn^{2+}. The contents of indium, sulfur, and zinc on the surface were quantified by In3d, S2p, and Zn2p peak areas, and the molar

Scheme 1. Proposed Morphology Formation Mechanism for the $ZnIn_2S_4$ Microspheres[a]

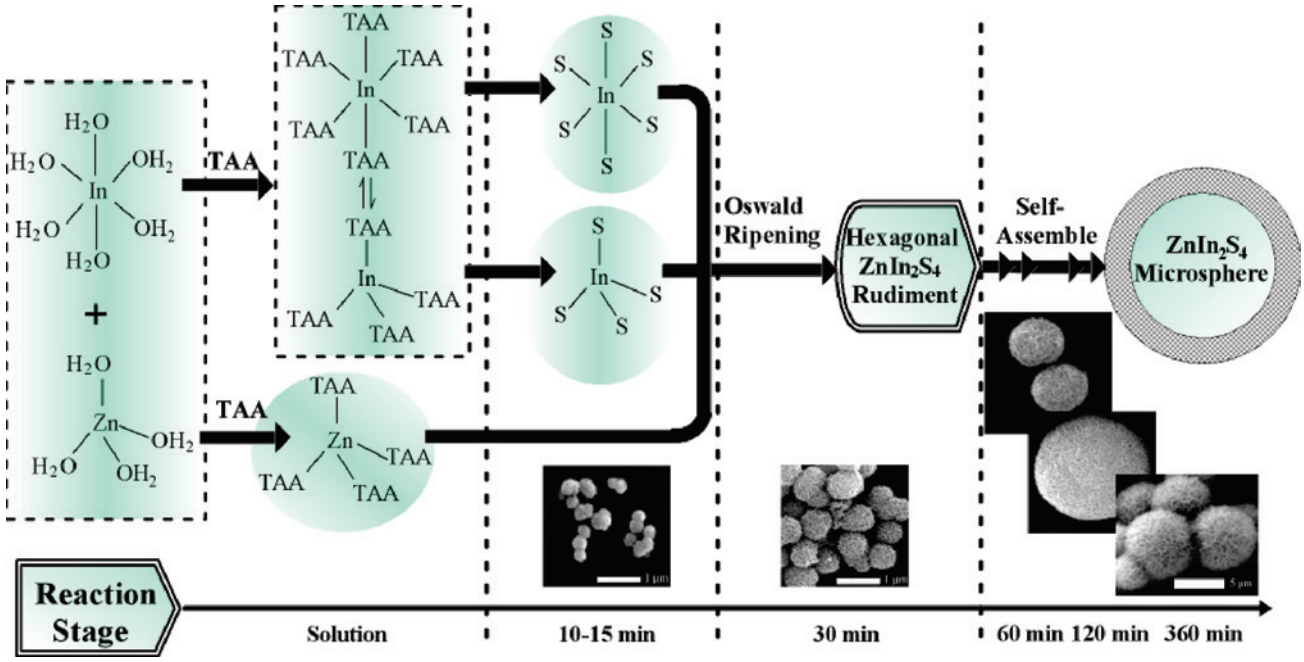

[a] Note: For clarity, the charges for the complexes (In, Zn, S) were omitted in the figure.

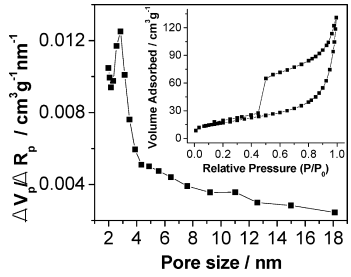

Figure 7. The pore size distribution plot and nitrogen adsorption−desorption isotherm (inset) of porous $ZnIn_2S_4$ microspheres.

ratio of 1.0:2.5:4.0 for Zn:In:S was given. No obvious peaks for other impurities were observed. Consequently, the as-synthesized products could be determined to be pure hexagonal phase $ZnIn_2S_4$ based on the results of XRD, EDS and XPS measurements. This indicated that crystalline $ZnIn_2S_4$ could be easily obtained under the current synthetic conditions.

Diffuse reflectance spectroscopy was a useful tool for characterizing the optical properties of materials. Figure 6 showed the UV−vis diffuse reflectance spectrum of as-prepared $ZnIn_2S_4$ powders. It could be seen that the $ZnIn_2S_4$ product has a steep absorption edge in the visible range, which indicated that the absorption relevant to the band gap was due to the intrinsic transition of the materials rather than the transition from impurity levels. Because the optical transitions of the $ZnIn_2S_4$ were similar to $CdIn_2S_4$, that was directly forbidden,[12] according to the equation $\alpha h\nu = A(h\nu - E_g)^2$ (where α, $h\nu$, and E_g were the absorption coefficient, the discrete photon energy, and the band gap energy, respectively; A was a constant),[13] a classical extrapolation approach was employed to estimate the E_g of $ZnIn_2S_4$ product. The plot of $(\alpha h\nu)^{1/2}$ versus $h\nu$ based on the direct forbidden was shown in the inset of Figure 6. The extrapolated value (the straight line to the X axis) of $h\nu$ at $\alpha = 0$ gave an absorption edge energy corresponding to $E_g = 2.2$ eV. This band gap energy corresponded to an optical absorption edge of 564 nm and was in agreement with the reported value of 2.3 eV.[6] The nitrogen adsorption−desorption isotherm of the porous $ZnIn_2S_4$ product was further investigated. As can be seen from Figure 7, the pore size distribution plot indicated that the diameter of the product was about 2−4 nm and the nitrogen adsorption−desorption isotherm (inset) was characteristic of a type IV isotherm with a hysteresis loop. They all indicated the presence of mesoporous structure in the product.[14,15] The BET surface area of the resulting $ZnIn_2S_4$ powder was 60.0 $m^2\ g^{-1}$. The porous structure and optical property would endow the as-prepared $ZnIn_2S_4$ microspheres with potential applications of effective photocatalysis.

To reveal the growth process of $ZnIn_2S_4$ microspheres, time-dependent experiments were carefully conducted. The products were collected at different stages during the reaction process from the reaction mixture, and then their morphologies were investigated by SEM and EDS. The images of the five typical products attained at 10, 15, 30, 60, and 120 min of reaction were displayed in Figure 8 respectively. As showed in part a of Figure 8, some small particles were attained at first, which have nearly circular shape with coarse surface. The corresponding EDS image (part g of Figure 8) indicated that the obtained sample contained a small amount

(12) Katsuki, S.-i. *J. Phys. Soc. Jpn.* **1972**, *33*, 1561–1565.
(13) Tsunekawa, S.; Fukuda, T.; Kasuya, A. *J. Appl. Phys.* **2000**, *87*, 1318–1321.
(14) Bavykin, D. V.; Parmon, V. N.; Lapkin, A. A.; Walsh, F. C. *J. Mater. Chem.* **2004**, *14*, 3370–3377.
(15) Gregg, S. J.; Sing, K. S. W. *Adsorption, Surface Area and Porosity*; Academic Press: London, 1982.

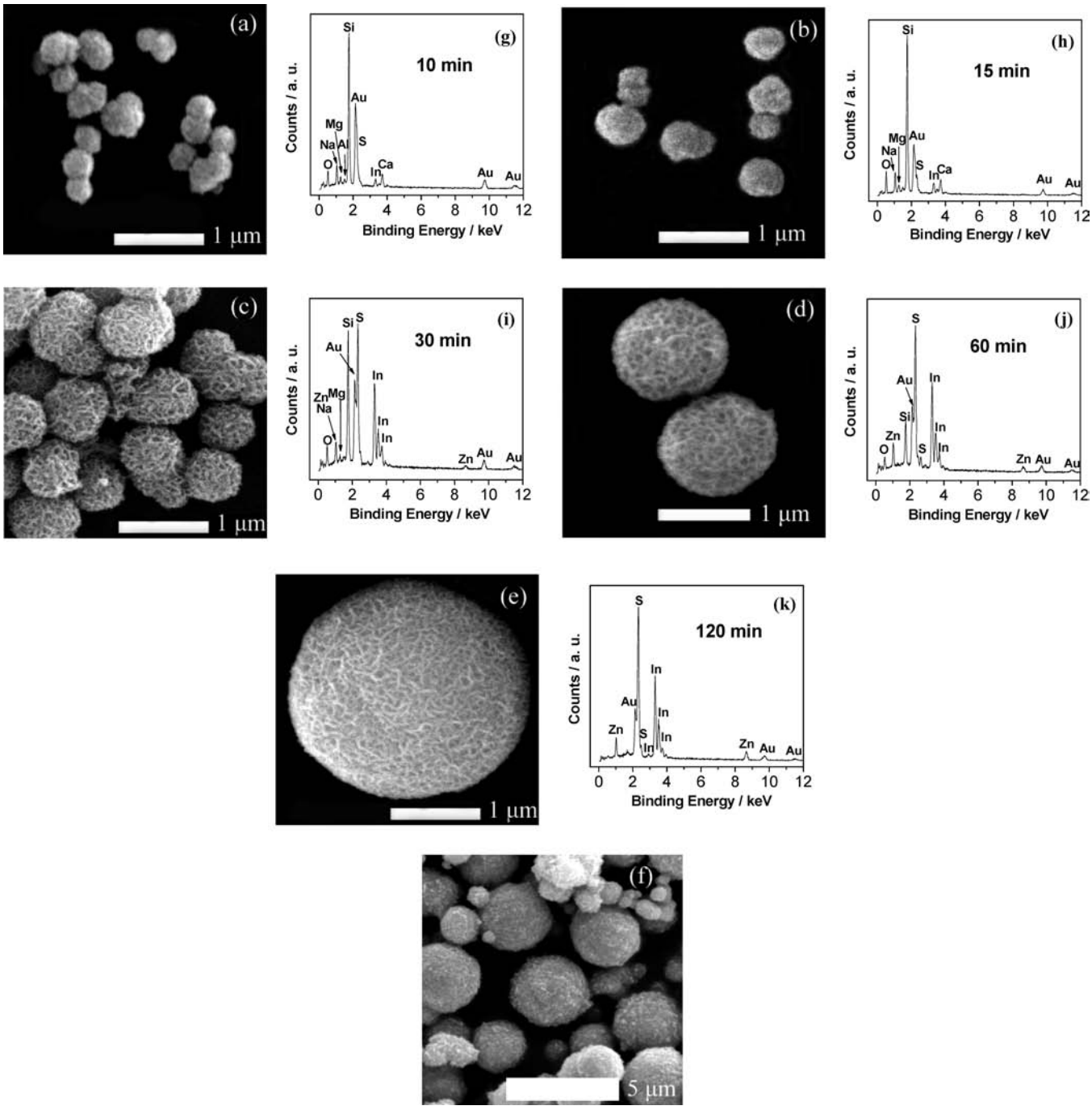

Figure 8. SEM and EDS images of the $ZnIn_2S_4$ products prepared at different heating time: 10 min for (a, g), 15 min for (b, h), 30 min for (c, i), 60 min for (d, j), and 120min for (e, k). The SEM image of the obtained In_2S_3 (f).

of indium and sulfur, except the oxygen, silicon, sodium, and so forth from the glass substrate and the gold came from the sputtered. As the reaction proceeded to 15 min (part b of Figure 8), the microspheres grew up. The 3.29 keV peak of indium in the corresponding EDS image (part h of Figure 8) was higher than that of part g of Figure 8, and a new 3.53 keV peak of indium appeared, whereas the peak of zinc was still absent. So, it could be speculated that the initial precipitation in the reaction system was the $In-S_x$ species. For the sake of demonstrating this consequence, the In_2S_3 was synthesized by TAA and $InCl_3$ through the same method. The morphologies of obtained In_2S_3 were investigated by SEM, showed in part f of Figure 8, which has similar outline and surface shape to those observed in parts a and b of Figure 8. After an additional 15 min, that is 30 min of the reaction, the microspheres further grew by the Oswald ripening process, and the microspheres that were combined by many nanosheets were obtained, as seen from part c of Figure 8. The corresponding EDS image, as showed in part i of Figure 8, indicated that the peaks of indium were higher than those of part h of Figure 8, and a new weak peak of zinc (8.67 keV) appeared. When the reaction time increased to 60 min, the microspheres grew to approximately 1 μm size, as displayed in part d of Figure 8. The peaks of zinc in EDS image (part j of Figure 8) were higher than those of part i of Figure 8. The microspheres then gradually grew, and the

unique structure almost appeared when the reaction time increased to 120 min (part e of Figure 8). The EDS image of 120 min, as shown in part k of Figure 8, was similar with Figure 4 that only contained the peaks of zinc, indium, sulfur, and sputtered gold. Finally, when the reaction was further prolonged to 6 h, the irregular particles were dissolved mostly, which resulted in the formation of unique microsphere structures, as demonstrated in part a of Figure 1.

In the synthesis of $ZnIn_2S_4$ microspheres, the pH value played an important role in determining the morphology of the products. Figure 9 displayed the SEM images of the samples prepared at pH 1 and 4. When the pH was about 4, $ZnIn_2S_4$ of ruleless dollops was produced rather than microspheres, as showed in part a of Figure 9. However, when the pH was lower than 0.5, there was limpid solution rather than any precipitation. The nanosheets congeries were obtained at pH 1 (part b of Figure 9), and the microsphere was gained at pH 2.5 (part b of Figure 1). This phenomenon was possibly due to the characteristic resolvability of TAA aqueous solution, which meant that the TAA was decomposed and the H_2S was released at a certain temperature in acidic aqueous solution. The decomposition rate of TAA was correlative with the amount of TAA, the pH value of solution, and the temperature of system. So, the exorbitant or lower pH value was not suited for the nanosheet structure, and the moderate pH 2.5 was suitable to the formation of $ZnIn_2S_4$ microspheres.

Furthermore, the influence of amount of TAA was investigated. The SEM images were displayed in Figure 10. It showed that the nanosheets and microspheres could not be produced when the TAA was 2 mmol (part a of Figure 10). Nevertheless, only the ruleless dollops were gained. When the TAA was 12 mmol (part b of Figure 10), the nanosheets and microspheres were produced, but the accumulated density of nanosheets was more serried than that of when TAA was 6 mmol (part b of Figure 1). This result was contributed to the thermal decomposition property of TAA, which was similar to the influence of pH value. The larger amount of H_2S gas was generated when the TAA was 12 mmol. As a consequence, the bubble of H_2S was more than that of when the TAA was 6 mmol, and the microspheres that were composed with more serried nanosheets, could be gained. When the TAA was 2 mmol, the bubble of H_2S was so few that the nanosheets could not be generated.

The visible-light photocatalytic activity of $ZnIn_2S_4$ product, and some comparative experiments were evaluated by degradation of MO aqueous solution. Under visible-light irradiation ($420\ nm < \lambda < 800\ nm$, the spectrum of combined filters was inset in part A of Figure 11), the photocatalytic results of MO were showed in part A of Figure 11. The y axis was defined as C/C_0 (where C was the main absorption peak intensity of MO at each irradiated time interval at wavelength of 464 nm and C_0 was the absorption intensity of starting 10 ppm MO solution). There was almost no degradation as the solution without any catalysts and with the nitrogen-doped titania (The amorphous TiO_2 xeogel, which was prepared by sol−gel method heated at 400 °C for 3 h under flowing NH_3 gas and then post annealed at

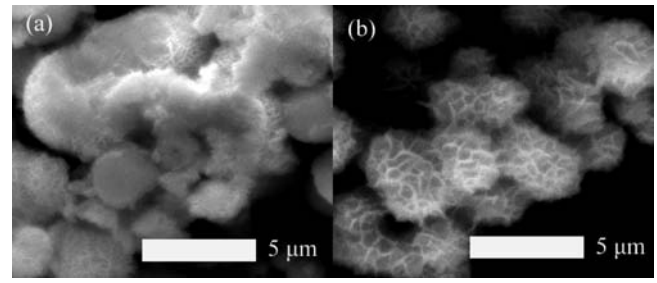

Figure 9. SEM images of the $ZnIn_2S_4$ products prepared at different pH: 4 for (a), and 1 for (b).

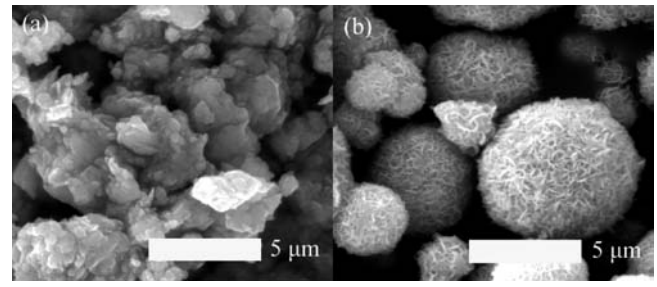

Figure 10. SEM images of the $ZnIn_2S_4$ products prepared at different amounts of TAA: 2 mmol for (a) and 12 mmol for (b).

400 °C for 2 h in static air to gain the $TiO_{2-x}N_x$ sample.[16]) under visible-light irradiation, which were displayed respectively as line a and line b. As showed in part A of Figure 11, line c, the absorption−desorption equilibrium was established after 30 min in dark absorption of $ZnIn_2S_4$ photocatalyst, so the light was turned on after 60 min of dark absorption. It could be clearly seen that, as showed in part A of Figure 11, line d, and part B of Figure 11, the MO was gradually photocatalytic degraded by porous $ZnIn_2S_4$ microspheres. After 2.5 h irradiation, the solution was nearly colorless, and the value of C/C_0 was about zero.

Discussion

$ZnIn_2S_4$ can be grown into two distinct polymorphs, either hexagonal or cubic lattices, depending on the synthetic method used.[17] A solution coordination model was previously proposed to explain the formation of cubic and hexagonal $ZnIn_2S_4$.[8−10] On the basis of the above-mentioned literatures and the experiment results, the growth mechanism of the as-synthesized $ZnIn_2S_4$ microspheres was proposed, as illustrated by Scheme 1. In solution, In^{3+} and Zn^{2+} with TAA could form three different complexes that were tetrahedral $[In(TAA)_4]^{3+}$, tetrahedral $[Zn(TAA)_4]^{2+}$, and octahedral $[In(TAA)_6]^{3+}$. Interestingly, there were some differences between our work and literatures. The description of literatures was that the $Zn-S_4$, $In-S_6$ and $In-S_4$ species generated at the same time and further combined in situ generated numerous $ZnIn_2S_4$ nuclei.[8−10] In the initial stage, the concentration of In^{3+} and Zn^{2+} were 0.02 and 0.01 mol/L respectively, and the concentrations of S^{2-} were identical. $In-S_6$ and $In-S_4$ species were formed and deposited first

(16) Chen, X. F.; Wang, X. C.; Hou, Y. D.; Huang, J. H.; Wu, L.; Fu, X. Z. *J. Catal.* **2008**, *255*, 59–67.
(17) Lopez-Rivera, S. A.; Mora, A. J.; Najarro, D. A.; Rivera, A. V.; Godoy, R. A. *Semicond. Sci. Technol.* **2001**, *16*, 367–371.

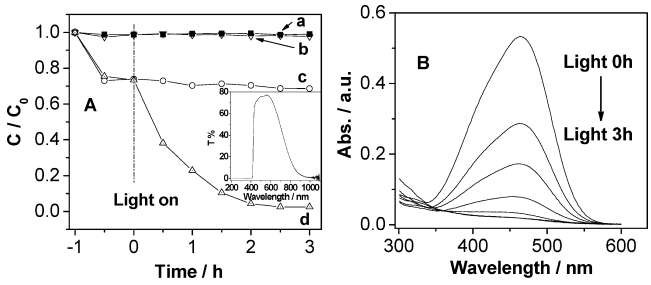

Figure 11. (A) Visible-light photocatalytic activities of MO for the $ZnIn_2S_4$ products: a) with light and without any catalyst, b) $TiO_{2-x}N_x$ with light, c) $ZnIn_2S_4$ in the dark, d) $ZnIn_2S_4$ with light. (Inset: the spectrum of combined filters.) (B) Time-dependent absorption spectral pattern of MO in the presence of $ZnIn_2S_4$ under the visible-light irradiation.

under thermal conditions, but $Zn-S_4$ species were not formed because the solubility product constant (K_{sp}) of In_2S_3 and ZnS were 5.7×10^{-74} and 1.51×10^{-21},[18,19] respectively. These results were confirmed by the EDS data (Figure 8) of 10 and 15 min samples. Meanwhile, these fresh generated $In-S_6$ and $In-S_4$ species underwent the process of Oswald ripening, and further combined with the $[Zn(TAA)_4]^{2+}$ in situ, resulting in a thermodynamically stable hexagonal $ZnIn_2S_4$ rudiment in which the coordination of In^{3+} ions were present in both the octahedral and the tetrahedral forms. Microspheres were further obtained with the continuous self-assemble of the building nanosheets. Regarding the formation of the marigold-like spherical structure, the geometric building nanosheets[20−22] might play a key role because no surfactants were used during the synthesis. A simple array of such crystal nanosheets would easily bend and develop into a marigold-like structure. The density of the nanosheets was further enhanced by the thermal conditions in the superfluous TAA reaction. However, the reason for such an unusual morphology has not been well understood. A similar type of morphology had been reported for $CdIn_2S_4$.[11] The results of this article are the development of the marigold-like binary metal sulfides. The details of the mechanism are currently under investigation.

(18) Sugimoto, T.; Chen, S. H.; Muramatsu, A. *Colloids Surf., A* **1998**, *135*, 207–226.
(19) Tuck, D. G. *Pure Appl. Chem.* **1983**, *55*, 1477–1528.
(20) Yang, J. L.; An, S. J.; Park, W. I.; Yi, G. C.; Choi, W. *Adv. Mater.* **2004**, *16*, 1661–1664.
(21) Liu, B.; Zeng, H. C. *J. Am. Chem. Soc.* **2004**, *126*, 16744–16746.
(22) Rautaray, D.; Sainkar, S. R.; Sastry, M. *Langmuir* **2003**, *19*, 888–892.

Conclusion

In summary, $ZnIn_2S_4$ microspheres of hexagonal crystal phase have been successfully synthesized by means of a facile thermal solution method. This method was a simple route that involved low temperature (353 K), no templates, no catalysts, no surfactants, or organic solvents. Therefore, it was very promising for low-cost and large-scale industrial production. A morphology formation mechanism has been proposed and discussed on the basis of experimental data. The porous $ZnIn_2S_4$ product showed enhancive visible-light photocatalytic activity. Other applications, such as solar energy conversion, environmental remediation, and advanced optical/electric nanodevices may also benefit from the unique properties of these porous $ZnIn_2S_4$ microspheres.

Acknowledgment. This work was financially supported by the National Natural Science Foundation of China (20537010, 20677010, and 20873023), An "863" Project From the MOST of China (2006AA03Z340), National Basic Research Program of China (973 Program: 2007CB613306), and the Natural Science Foundation of Fujian, China (2003F004 and 2005HZ1007). We also gratefully thank Dr. Yilin Chen, Yidong Hou and Qingping Wu for helpful discussion.

IC800752T